

Cholesterol 25-hydroxylase (CH25H) as a promoter of adipose tissue inflammation in obesity and diabetes



Lucia Russo¹, Lindsey Muir¹, Lynn Geletka¹, Jennifer Delproposito¹, Nicki Baker², Carmen Flesher², Robert O'Rourke², Carey N. Lumeng^{1,3,*}

ABSTRACT

Objective: Expansion of visceral adipose tissue (VAT) and metabolic inflammation are consequences of obesity and associated with type 2 diabetes (T2DM). Metabolically activated adipose tissue macrophages (ATMs) undergo qualitative and quantitative changes that influence their inflammatory responses. How these cells contribute to insulin resistance (IR) in humans is not well understood. Cholesterol 25-Hydroxylase (CH25H) converts cholesterol into 25-Hydroxycholesterol (25-HC), an oxysterol that modulates immune responses. Using human and murine models, we investigated the role of CH25H in metabolic inflammation.

Methods: We performed transcriptomic (RNASeq) analysis on the human whole AT biopsies and sorted ATMs from obese non-diabetic (NDM) and obese diabetic (DM) subjects to inquire if *CH25H* was increased in DM. We challenged mice lacking *Ch25h* with a high-fat diet (HFD) to characterize their metabolic and immunologic profiling. *Ch25h* KO mice and human adipose tissue biopsies from NDM and DM subjects were analyzed. LC-MS was conducted to measure 25-HC level in AT. In vitro analysis permitted us to investigate the effect of 25-HC on cytokine expression.

Results: In our RNASeq analysis of human visceral and subcutaneous biopsies, gene pathways related to inflammation were increased in obese DM vs. non-DM subjects that included *CH25H*. CH25H was enriched in the stromal vascular fraction of human adipose tissue and highly expressed in CD206⁺ human ATMs by flow cytometry analysis. We measured the levels of the oxysterols, 25-HC and 7 α 25diHC, in human visceral adipose tissue samples and showed a correlation between BMI and 25-HC. Using mouse models of diet-induced obesity (DIO), we found that HFD-induced *Ch25h* expression in eWAT and increased levels of 25-HC in AT. On HFD, *Ch25h* KO mice became obese but exhibited reduced plasma insulin levels, improved insulin action, and decreased ectopic lipid deposit. Improved insulin sensitivity in *Ch25h* KO mice was due to attenuation of CD11c⁺ adipose tissue macrophage infiltration in eWAT. Finally, by testing AT explants, bone marrow-derived macrophages (BMDMs) and SVF cells from *Ch25h* deficient mice, we observed that 25-HC is required for the expression of pro-inflammatory genes. 25-HC was also able to induce inflammatory genes in preadipocytes.

Conclusions: Our data suggest a critical role for CH25H/25-HC in the progression of meta-inflammation and insulin resistance in obese humans and mouse models of obesity. In response to obesogenic stimuli, CH25H/25-HC could exert a pro-inflammatory role.

© 2020 The Authors. Published by Elsevier GmbH. This is an open access article under the CC BY-NC-ND license (<http://creativecommons.org/licenses/by-nc-nd/4.0/>).

Keywords CH25H; Oxysterol; Obesity; Diabetes; Adipose tissue; Macrophage

1. INTRODUCTION

Obesity is considered a global epidemic that dramatically affects general population health [1,2] due to its association with type 2 diabetes (T2DM) and metabolic syndrome (MetS) [3–5]. A substantial body of evidence suggests that obesity-induced inflammation links obesity metabolic diseases, such as DM [6]. There is substantial variation in this association, however, as up to 70% of obese subjects

remain metabolically healthy based on insulin resistance (IR) and DM status [7]. The difference in inflammatory gene expression in adipose tissue has been shown to differentiate metabolically healthy obese subjects without DM from those that are metabolically unhealthy. A hallmark of metabolic-inflammation is the contribution of activated adipose tissue macrophages (ATMs) to disease progression. ATMs can adopt a metabolic activation state with prominent lysosomal activity [8–10], secrete pro-inflammatory cytokines [11,12], and act as

¹Department of Pediatrics, Division of Pulmonary Medicine, University of Michigan Medical School, Ann Arbor, MI, United States ²Department of Surgery, University of Michigan Medical School, Ann Arbor, MI, United States ³Molecular and Integrative Physiology, University of Michigan Medical School, Ann Arbor, MI, United States

*Corresponding author. University of Michigan Medical School, 2057 Biomedical Science Research Building (BSRB), 109 Zina Pitcher Place, Ann Arbor, MI, 48109-2200, United States. E-mail: clumeng@umich.edu (C.N. Lumeng).

Abbreviations: CH25H, Cholesterol-25-Hydroxylase; 25-HC, 25-Hydroxycholesterol; WT, *Ch25h* wild-type mice; KO, Global *Ch25h* homozygous null mutant mice; *Ch25h*, Gene encoding Ch25h enzyme in mice; *CH25H*, Gene encoding CH25H enzyme in humans; AT, Adipose tissue; eWAT, epididymal white adipose tissue; SVF, Stromal vascular fraction; ATM, Adipose tissue macrophage; IR, Insulin resistance; T2DM, Type 2 Diabetes; NDM, Obese non-diabetic subjects; DM, Obese diabetic subjects

Received January 20, 2020 • Revision received March 9, 2020 • Accepted March 20, 2020 • Available online 27 March 2020

<https://doi.org/10.1016/j.molmet.2020.100983>

antigen presenting cells (APCs) [13–15] to disrupt adipose tissue (AT) metabolism during obesity [16].

While numerous inflammatory pathways have been implicated in ATM activation, we have focused on the potential contribution of Cholesterol 25-hydroxylase (CH25H). CH25H catalyzes the formation of 25-hydroxycholesterol (25-HC) from cholesterol and contributes to the first steps in bile acid and oxysterol synthesis pathways [17]. CH25H was identified as a member of the macrophage-enriched metabolic network (MEMN) in adipose tissue [18] and was upregulated in visceral adipose tissue (VAT) of obese subjects and downregulated with weight loss post-bariatric surgery [19]. Under normal conditions, most tissues and cells express CH25H at low levels. However, CH25H is strongly induced, along with 25-HC, by Toll-like receptors (TLR) [20,21], interferon receptor (IFNR) [22,23], and LXR activation in macrophages [24], suggesting a link between metabolic and inflammatory pathways through CH25H. NFKB's inhibitors, curcumin and resveratrol, were shown to block induced CH25H overexpression [25]. CH25H upregulation has been reported in multiple tissues in disease settings (liver, lung, colon, intestine, brain, kidney, spleen, heart, thymus, skin and muscle), but few studies have addressed CH25H expression in adipose tissue.

Previous studies have investigated the role of Ch25h in viral infection models and assigned to Ch25h/25-HC a role as an antiviral agent in host defense [25,26]. Ch25h KO mice were shown to be more susceptible to MHV68 lytic [25] and gamma-herpes virus infection [22]. An independent study reported that following influenza infection, Ch25h KO mice remained more protected compared to controls, showing less severe lesions in lungs and attenuated inflammatory responses [21]. This latter evidence suggested that Ch25h/25-HC is required to amplify inflammatory responses in macrophages following activation with TLR3 agonist and with other pattern-recognition receptor (PRR) ligands, including Myd88-dependent TLR7 and TLR9, and the intracellular receptor NLRP3 [21].

The immunological phenotype of regular diet (RD) fed Ch25h KO mice was described in another study [25]. This group reported that Ch25h KO mice were featured with increased levels of IgA in sera, lungs, and mucosa, and 25-HC repressed IgA secretion in vitro. However, no changes in the numbers of total white blood cells, neutrophils, lymphocytes, monocytes, eosinophils, basophils, B-cells, T cells, and macrophages were found in the blood. The number of B-cells, T cells, macrophages, and neutrophils was not different in lung and spleen [25]. To us, the limit of this study was that immune cells were not evaluated in adipose tissue.

Currently, the knowledge about the implication and function of Ch25h in metabolic regulation in mice is limited. Evidence demonstrated that the adenovirus-mediated overexpression of Ch25h in the liver led to improved insulin sensitivity in WT mice [27]. On the other hand, Ch25h loss was implicated in the protection from obesity/metabolic disease seen in stagger (sg) mice [28,29]. In a recent paper, Ch25h KO mice were administered with a high-cholesterolemic diet (HCD) and subjected to a model of metabolism associated post-traumatic osteoarthritis (OA). This study showed reduced OA manifestations in these mice but their metabolic and immunological profiling was not described [30].

The goal of our study was to address the unresolved contribution of CH25H to metabolic disease in the setting of obesity-induced adipose tissue inflammation. We identified an association between CH25H and DM status. Herein, we hypothesized that increased levels of CH25H/25-HC could exert a detrimental effect on the regulation of meta-inflammation. To address our hypothesis, we characterized the immunological and metabolic profile of Ch25h KO mice fed an HFD. We

found that obese Ch25h KO mice exhibited improved insulin resistance and features of reduced adipose tissue inflammation due to the attenuation of CD11c⁺ macrophage accumulation in adipose tissue. By in vitro analysis, we evaluated the effect of the ablation and reconstitution of 25-HC level on the induction of pro-inflammatory cytokine expression in response to inflammatory mediators.

2. MATERIAL AND METHODS

2.1. Human and murine adipose tissue preparation and RNA seq analysis

Visceral (VAT, greater omentum) and subcutaneous adipose tissue (SAT, abdominal wall) were collected from bariatric surgery patients enrolled with Institutional Review Board approval at the University of Michigan and Ann Arbor Veteran's Administration Hospital. (Demographics in Table 1). Patients were matched for age and BMI and stratified per ADA criteria: diabetic (DM) subjects were defined by clinical diagnosis requiring medication and HbA1c >= 6.5; non-Diabetic (NDM) subjects had no clinical history of DM, no DM-related medication use, and HbA1c < 5.7. Total RNA was extracted (Qiagen), polyA enriched, and subjected to RNA sequencing by the UM DNA Sequencing Core, using the Illumina Hi-Seq platform (>80 reads/sample). Data analysis used FastQC (version 0.10.0) and the Tuxedo Suite package for alignment, differential expression analysis, and post-analysis diagnostics aligned to the UCSC hg19 reference genome using TopHat, Bowtie, and Cufflinks/CuffDiff. Data visualization and pathway analysis was performed with iPathwayGuide (Avaita). DE gene threshold at LogFC > 0.5 and padj < 0.05 GSEA analysis was performed with the Java installation. Graphs were generated with ggplot2.

2.2. Real-time quantitative PCR (qRT-PCR) and immunoblotting

For Real-time PCR, RNA from tissues and cells was prepared using RNeasy Midi Kits (QIAGEN), and cDNA was generated using high capacity cDNA reverse transcription kits (Applied Biosystems). Real-time RT-PCR analyses were done in duplicate on the ABI Step-one-plus Sequence Detection System (Applied Biosystems) with the SYBR Green PCR kit, as instructed by the manufacturer (Applied Biosystems). Relative expression was assessed by the comparative CT method correcting for the amplification efficiency of the primers and performed in duplicate. A check for unspecific products was conducted by performing a post-amplification melting curve analysis. Normalization was done by normalizing threshold cycles (Ct values) to PPIA (human genome) or ARBP1 (mouse genome) within each sample for obtaining Δ Ct values sample-specific (= Ct gene of interest - Ct housekeeping gene). Fold expression levels were obtained by calculating $2^{-\Delta\Delta Ct}$ levels ($\Delta\Delta Ct = \Delta Ct$ treatment - ΔCt control). Primers used are indicated in ESM Table 2. Methods are also reported previously [31]. For Immunoblotting, the protocol is reported in previous publication [32]. Antibodies used for immunoblotting included an anti-human/mouse Ch25h primary antibody (Hybridoma G18 mouse anti-human CH25H, kindly provided by Dr. Russell from UT South Western) and

Table 1 — Subject Demographics for RNA Sequencing Analysis.

	Non-DM (n = 10)	DM (n = 10)	p-value
Sex (% female)	50	50	
Age (y)	40.4 ± 11.8	46.6 ± 11.0	0.057
BMI (kg/m ²)	48.31 ± 7.6	48.44 ± 6.3	0.946
HbA1c (%)	5.61 ± 0.32	6.92 ± 1.21	0.0006
Fasting Glucose (mg/dL)	88.2 ± 9.2	134.4 ± 49.2	0.0038

a polyclonal antibody against beta-Actin antibody (Cell Signaling), which was used for normalization. The intensity of each band was measured from digital scans of each membrane using ImageJ.

2.3. Immunofluorescent stain and H-E stain

For *Immunofluorescence*, the stain was performed as described previously [33] using the following antibodies: anti-Mac2 (M3/38), and anti-CH25H (Hybridoma G18 kindly provided by Dr. David Russell from UT South-Western). TXRED Alexa Fluor 568 Goat anti-rat secondary Ab (Life Technology), for channel 568 nm to detect rat primary Ab anti-MAC-2, and INFRARED Alexa Fluor 647 APC Goat anti-mouse secondary Ab (Invitrogen), for channel 647 nm to detect mouse primary Ab anti-CH25H, were used. Samples were incubated with BODIPY (Thermo Scientific) followed by incubation with DAPI (Life Technologies) to detect adipocytes and nuclei, respectively. Images were collected using an Olympus Fluoview 100 laser scanning confocal microscope (Leica LX5 Microsystems).

For *H&E*, Formalin-fixed, paraffin-embedded epididymal white adipose tissue and liver sections were stained with hematoxylin-eosin (H&E). Pictures were obtained using ImageJ software.

For *adipocyte sizing*, the protocol is described in previous publications [34].

2.4. SVF isolation and flow cytometry analysis

In *human adipose tissue*, SVF cells were isolated as described previously [34]. Antibodies included the following: CD45-PerCp Cy5.5 (Bioscience), CD64-PE, CD11c-PE Cy7, CD206-APC Cy7 (Biolegend), CH25H (Hybridoma G18 kindly provided by Dr. David Russell from UT South Western), and an anti-rabbit secondary INFRARED Alexa Fluor 647 APC antibody (Invitrogen). Live/dead fixable violet staining kits (Life Technology) were used according to the manufacturer's instruction.

In *mouse samples*, spleen cells were collected after crushing the spleen through a 70 μ m cell strainer and spinning samples briefly. Red blood cells were lysed in Red Blood Cell Lysis (RBC) buffer before blocking. Cells were washed, spun and resuspended in RPMI media. A representative volume of cells was counted using the Accuri instrument. 500 μ l of cells for each sample was spun before flow cytometry staining. Adipose tissue SVF cells were isolated as described previously [35]. Cells were incubated in FC Block Anti-mouse CD16/CD32 (eBioscience) for 10 min on ice and stained with indicated Abs for 30 min at 4 °C. Staining protocols with antibody clones as reported in previous publications [31,32,35,36]. Abs used for flow staining are as follows: CD45.2 e450 for leukocytes; CD64 PE (BD Pharmagen), CD11c APC-Cy7 and CD11b PE-Cy7 (eBioscience) for ATMs; CD3 PerCyanine5.5, CD4 APC, and CD8 FITC (eBioscience) for T cells.

Fluorescence minus one controls were included in all human and mouse experiments. All samples were analyzed by Fortessa flow cytometer and data using FlowJo software (Tree Star Inc., Ashland, OR, USA) after the exclusion of doublets and non-viable cells using fluorescence-minus-one controls with forward scatter/side scatter gates encompassing all cells with subsequent analysis of CD45⁺ cells.

2.5. 25-HC and 7 α ,25-di-HC measurement

A sensitive and accurate method was developed for the quantitation of 25-HC and 7 α ,25-di-HC cholesterol in adipose tissue (eWAT) by utilizing Oxysterol Derivatization MaxSpec Kit combined with liquid chromatography-tandem mass spectrometry (LC-MS/MS) in collaboration with Cayman Technology (Ann Arbor). Each sample was weighed and homogenized in PBS at a weight (g) to volume (mL) ratio of 1:10. Adipose tissue samples, including visceral omental adipose

tissue from human subjects (Demographics in [ESM Table 3](#)) and epididymal white adipose tissue from WT and *Ch25h* KO mice, were homogenized using the Precellys Evolution homogenizer. Calibration standard and Quality Control samples were precipitated with ethanol containing 40 ng/ml of d6-25-hydroxy cholesterol. Extracted oxysterols were oxidized and using Oxysterol Maxspec kit, according to the instructions. Detection of oxysterols was achieved by enzyme-assisted derivatization using Girard P reagent, which contains a positively charged quaternary nitrogen group. The Girard P reagent derivatized calibration standards and QC samples were cleaned and enriched using Waters Oasis HLB 96 wells plate. All the calibration standards and QC samples were diluted with an equal volume of water before sample loading. Afterward, the derivatized oxysterols were washed with 10% and 30% MeOH on the cartridges before elution. The combined eluate was processed under-speed vacuum. Each sample was resuspended into MeOH for LC-MS/MS. To quantify 25-HC and 7 α , 25diHC in the samples, calibration curves of each analyte were prepared in a 4% BSA matrix over a linearity range of 0.25 ng/ml –100 ng/ml. In the assay, the concentration of 25-HC and 7 α 25diHC was normalized to protein content in each homogenate. For protein quantitation, each homogenate was diluted with Millipore water and assayed using the Cayman's Protein Determination Kit. A standard curve was established by dilution of the BSA standard between 5.6 and 32 μ g/ml using Millipore water as the matrix. The concentration of each sample was calculated from a polynomial fit of the standard concentration versus absorbance. Data show the concentration of 25-HC and 7 α 25diHC per wet eWAT.

2.6. Experimental mice

Ch25h KO mice [25] were purchased from Jackson Laboratories (JAX stock #016263). *Ch25h* C57BL/6J WT were also purchased from Jackson Laboratories (JAX stock #000664) and used as controls. Mice from both genotypes were bred for experiments. Spot genotyping was performed by PCR-based genotyping using ear genomic DNA and primers for the WT and the KO allele. Genotyping protocols were provided by Jackson lab (available on Jack lab website). Mice for experiments (except when indicated otherwise) were male and were fed ad libitum either a control regular chow diet (RD; LabDiet PicoLab 5001; 4.09 kcal/gm; 28.5% protein, 13.5% fat; 57.9% carbohydrate) or a high-fat diet (HFD; Research Diets D12492; 5.24 kcal/gm 20% protein; 60% kcal fat; 20% carbohydrate) starting at 9-weeks of age for 12-week duration. Experiments to evaluate the metabolic and immunological profiling of *Ch25h* KO mice administered an HFD and were conducted in three independent cohorts of age-matched WT and KO mice with similar findings. The final experiment was conducted on littermates (N = 8–10/group). Animals were housed in a specific pathogen-free facility with a 12-hour light/12-hour dark cycle and given free access to food and water. Mice were sacrificed at fed state by cervical dislocation and tissue samples were collected, immediately snap-frozen in liquid nitrogen, and stored at –80 °C until further analysis. Animal protocols were in compliance with the Institute of Laboratory Animal Research Guide for the Care and Use of Laboratory Animals and approved by the University Committee on Use and Care of Animals at the University of Michigan (animal welfare assurance number A3114-01).

2.7. Metabolic profiling

For *glucose and insulin tolerance test*, following a 6-hour fast, mice were given glucose (1 g/kg) or regular human insulin (0.75 U/kg Actrapid; Novo Nordisk) via intraperitoneal (ip) injection. At the indicated time points (0, 15, 30, 45, 60, 90, 120 and 180 min), blood

drops for determination of glucose levels were collected from the tail vein. An Accu-Chek (Roche) glucometer was used for assessing glycemia. Protocols are reported in a previous publication [37]. For *metabolic evaluation*, bodyweights were measured weekly. Nuclear Magnetic Resonance (Bruker Minispec) was used to determine fat, lean and fluid mass in HFD-fed mice (see [ESM Table 4](#)). Blood glucose was measured by glucometer, at fed stated, and at fasting state after an overnight-fasted period. Jugular venous blood was drawn at 1100 h from overnight-fasted mice to measure plasma insulin and NEFA levels. Levels of NEFA were evaluated by the Wako Diagnostics kit. Levels of insulin in plasma were measured using a commercially available ELISA (CristalKem), according to the manufacturer's instructions. Methods are reported in a previous publication [31].

2.8. Treatment of adipose tissue explants, SVF cells, bone marrow-derived macrophages, 3T3-L1 cells and human preadipocytes

Epididymal white adipose tissue pads were excised from RD-fed WT and *Ch25h* KO mice, divided into equal pieces and transferred into 12-well plates in the presence of DMEM media. They were incubated with either vehicle alone (Veh) or with lipopolysaccharide (LPS 100 ng/ml for 8 h) or with tumor necrosis factor- α (10 ng/ml for 8 h) alone or combined ($n = 3$ wells/genotype/treatment). Explants were washed before mRNA being extracted. A similar experiment was also conducted in eWAT-derived SVF cells. SVF cells were counted and plated at a concentration of 1×10^6 cells/ml in DMEM media prior to treatment with lipopolysaccharide (LPS 100 ng/ml for 8 h) or with 25-HC (10 μ g/ml for 8 h) alone or combined ($n = 3$ wells/genotype/treatment). For the isolation of BMDMs, femurs from RD-fed WT and *Ch25h* KO mice were used to flush cells from the bone marrow cavity. Marrow was broken up by aspiration. Cells were spun and lysed in an RBC lysis buffer. Cell pellets were resuspended in DMEM + 10% FBS HI-CERT + 20% L929 media. Cells were counted and plated at a concentration of 1×10^6 cells/ml in differentiation media, which was replaced every 2 two days until day 7, when it was changed to DMEM + 10% FBS HI-CERT media. Not differentiated 3T3-L1 cells were kept in DMEM media enriched with Newborn Calf Serum and human preadipocytes in DMEM media with 15% FBS prior to treatment. *Treatment with LPS and Tnf α* : Cells were treated with either vehicle alone (Veh) or with lipopolysaccharide (LPS 100 ng/ml for 8 h) or with Tnf α (10 ng/ml for 8 h) alone or combined to LPS ($n = 3$ wells/genotype/treatment). Cells were washed in PBS before the mRNA extraction. *Treatment with LPS and 25-HC*: Tnf α was replaced with 25-HC (25-HC 5 μ g/ml for 8 h) alone or combined to LPS.

2.9. Statistical analysis

All data were graphed and analyzed using Prism8 (GraphPad Software, Inc.) Data are presented as Mean \pm SEM. The comparison was performed for WT versus *Ch25h* KO differences within each diet or for diet groups within each group, respectively. Statistical differences were assessed using a two-tailed t-test or ANOVA (with Tukey's post-test analysis). Differences were considered significant when $p < 0.05$.

3. RESULTS

3.1. Human VAT and SAT from obese DM subjects are enriched for inflammatory gene pathways

Few studies have used RNA sequencing to compare gene expression from diabetic (DM) and non-DM (NDM) individuals. VAT and SAT samples from obese DM and NDM subjects matched for age and BMI (10 females and 10 males per group) underwent RNAseq analysis followed by a differential expression (DE) gene and pathway analysis

([Figure 1A–B](#)). Initial analysis comparing depot-specific DE genes between DM and NDM individuals identified 161 genes (118 increased) in VAT and 463 genes (334 increased) in SAT with 65 genes in common between both depots. Pathway and GSEA analysis demonstrated a significant perturbation of the genes involved in hematopoietic cell lineage, phagosome, chemokine signaling, and cytokine–cytokine receptor interaction in VAT and pathways related to complement and coagulation cascades, systemic lupus erythematosus, and AGE-RAGE signaling in SAT ([ESM Fig. 1](#) and [ESM Table 1](#)). Disaggregation of the data by sex demonstrated sex-specific DE genes that depended on the depot sampled ([Figure 1B](#)). Pathway analysis again demonstrated significant enrichment of genes related to inflammatory responses that varied between depot and sex ([Figure 1C](#)). In our cohort, female VAT had the largest enrichment of DE genes related to inflammation between DM and NDM individuals.

3.2. *CH25H* mRNA is upregulated in visceral adipose tissue from obese diabetic subjects and is enriched in human ATMs

To identify novel genes of interest related to inflammation, we interrogated the set of genes that were induced in DM individuals independent of depot and sex ([Figure 1D](#)). One of the genes observed to be elevated in DM vs. NDM VAT in both males and females was Cholesterol 25-hydroxylase (*CH25H*). We confirmed the RNAseq finding of a *CH25H* mRNA induction in DM VAT in an independent set of samples from male subjects ([Figure 2A](#)). The expression of *CH25H* in obese DM males was higher than lean or obese NDM VAT. A similar trend was seen in VAT from obese women with DM. Gene expression of stratified VAT showed that *CH25H* is highly expressed in SVF cells compared to mature adipocytes in human VAT ([Figure 2B](#)). Immunoblots demonstrated elevated CH25H protein in VAT in DM compared to NDM in both men and women ([Figure 2C](#)). To identify the primary cells expressing CH25H in VAT, we used intracellular flow cytometry. CH25H was detected in CD206⁺ hATMs and was increased compared to CD206⁻ hATMs ([Figure 2D](#)). Immunofluorescence analysis of whole-mount VAT biopsies demonstrated localization of CH25H in MAC2⁺ hATMs ([Figure 2E](#)). Overall, these studies demonstrate that CH25H is enriched in ATMs and is elevated in obese DM patients compared to NDM. Levels of 25-HC and 7 α 25diHC measured by LCMS analysis in VAT samples of NDM and DM male subjects were not significantly different between groups ($N = 10$) ([Figure 2F](#)). We hypothesize that this may be due to metabolism of 25-HC in adipose tissue or CH25H independent sources of 25-HC production. Correlational analysis between oxysterol levels and subject demographics (age, BMI and HbA1c) showed a significant R-squared coefficient between 25-HC and BMI in our cohort ([Figure 2F](#)). Correlations relative to age, HbA1c and *CH25H* expression were also assessed, but no statistically significant associations were observed ([ESM Fig. 5](#)).

3.3. High-fat diet induces *Ch25h* mRNA and 25-HC production in mouse eWAT

Given the limited studies on *Ch25h* and 25-HC in obese adipose tissue, we examined the effect of diet-induced obesity in *Ch25h* KO mice. We fed an RD (13.5% fat) and an HFD (60% fat) chow to *Ch25h* KO and WT male mice for 12 weeks. Bodyweight (BW) was similar between RD groups, although *Ch25h* KO mice were slightly lighter than *Ch25h* WT at an early age ([Figure 3A](#)). On HFD, both genotypes gained weight ([Figure 3A](#)). *Ch25h* KO mice showed a slightly lighter BW compared to HFD-fed *Ch25h* WT mice. Despite this, fat and lean mass measured by nuclear magnetic resonance (NMR) in HFD fed mice were not significantly different between genotypes ([ESM Table 4](#)). No significant differences in BW were observed between female WT and *Ch25h* KO

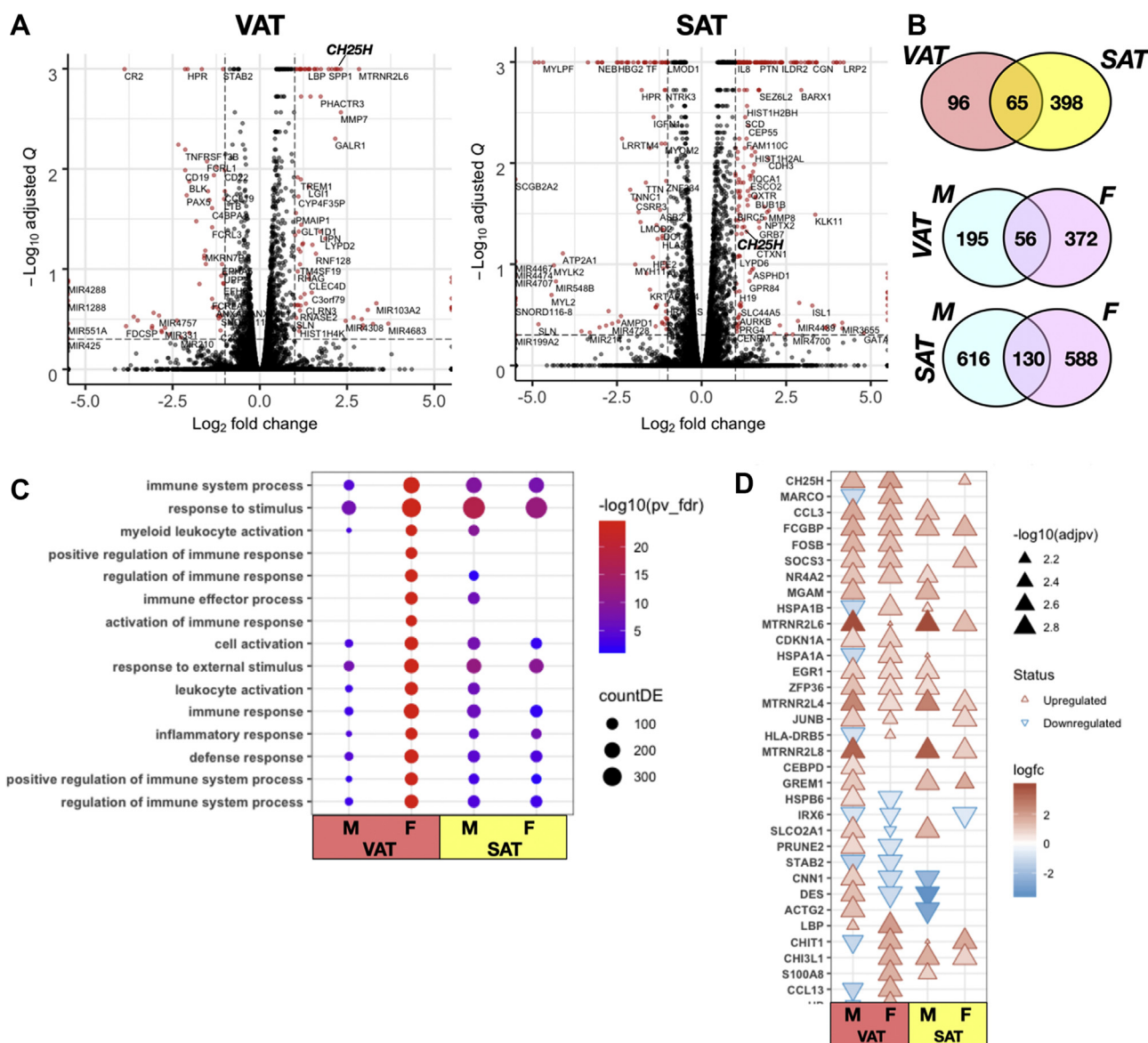


Figure 1: Data from mRNA sequencing analysis in human visceral omental and subcutaneous adipose tissue of obese and diabetic subjects. **A)** Volcano plot of differentially expressed genes (DEGs) in VAT and SAT from human obese and diabetic male and female subjects ($N = 5/\text{group}/\text{sex}$). Subject demographics is provided in [Table 1](#). The data of all genes are plotted as \log_2 fold change versus the $-\log_{10}$ of the adjusted p-value. Thresholds are shown as dashed lines. Genes selected as significantly different are highlighted as red dots. Note the prominent position of the *CH25H* gene, which was chosen for further analysis. **B)** The Venn diagrams show the numbers of DEGs in common or specific between the VAT and SAT (upper) and distributed between males and females (lower). **C)** Gene Ontology (GO) and Enriched Kyoto Encyclopedia of Genes and Genomes (KEGG) pathway analyses of the most significantly enriched biological processes (adjusted p-value < 0.05 , Benjamini-Hochberg) linked to the DEGs in VAT and SAT distributed between male and female subjects. Significant terms are associated with activation of immune system responses. The complete list of analyses of DEGs distributed by depot and sex is provided in [ESM Table 1](#). **D)** Heat-map showing the \log_2 fold change in expression of the DEGs involved in biological processes and KEGG pathways associated with immune system activation. Note the upregulation of the *CH25H* gene in VAT.

mice fed HFD ([ESM Fig. 2A](#)). To examine the effect of HFD on *Ch25h* expression in adipose tissue, we measured the mRNA level of WT and *Ch25h* KO mice. HFD significantly induced *Ch25h* mRNA expression in epididymal white adipose tissue (eWAT) ([Figure 3B](#)). As expected, *Ch25h* mRNA was absent in KO mice. We next measured levels of 25-HC in response to HFD in eWAT. 25-HC and $7\alpha,25\text{diHC}$ were present at a low level in lean RD-fed WT mice and were significantly lower in *Ch25h* KO mice. HFD feeding increased the concentrations of 25-HC

([Figure 3C](#)) and $7\alpha,25\text{diHC}$ ([Figure 3D](#)) in eWAT in obese WT mice compared to lean controls. In HFD fed *Ch25h* KO mice, 25-HC and $7\alpha,25\text{diHC}$ were both significantly decreased compared to WT mice but were still detectable at levels comparable to lean KO mice. The decrease in 25-HC amount in *Ch25h* KO mice was more prominent than $7\alpha,25\text{diHC}$. This demonstrates that HFD-mediated obesity induces *Ch25h* and 25-HC production in adipose tissue and that 25-HC generation, but not $7\alpha,25\text{diHC}$, is directly dependent on *Ch25h*.

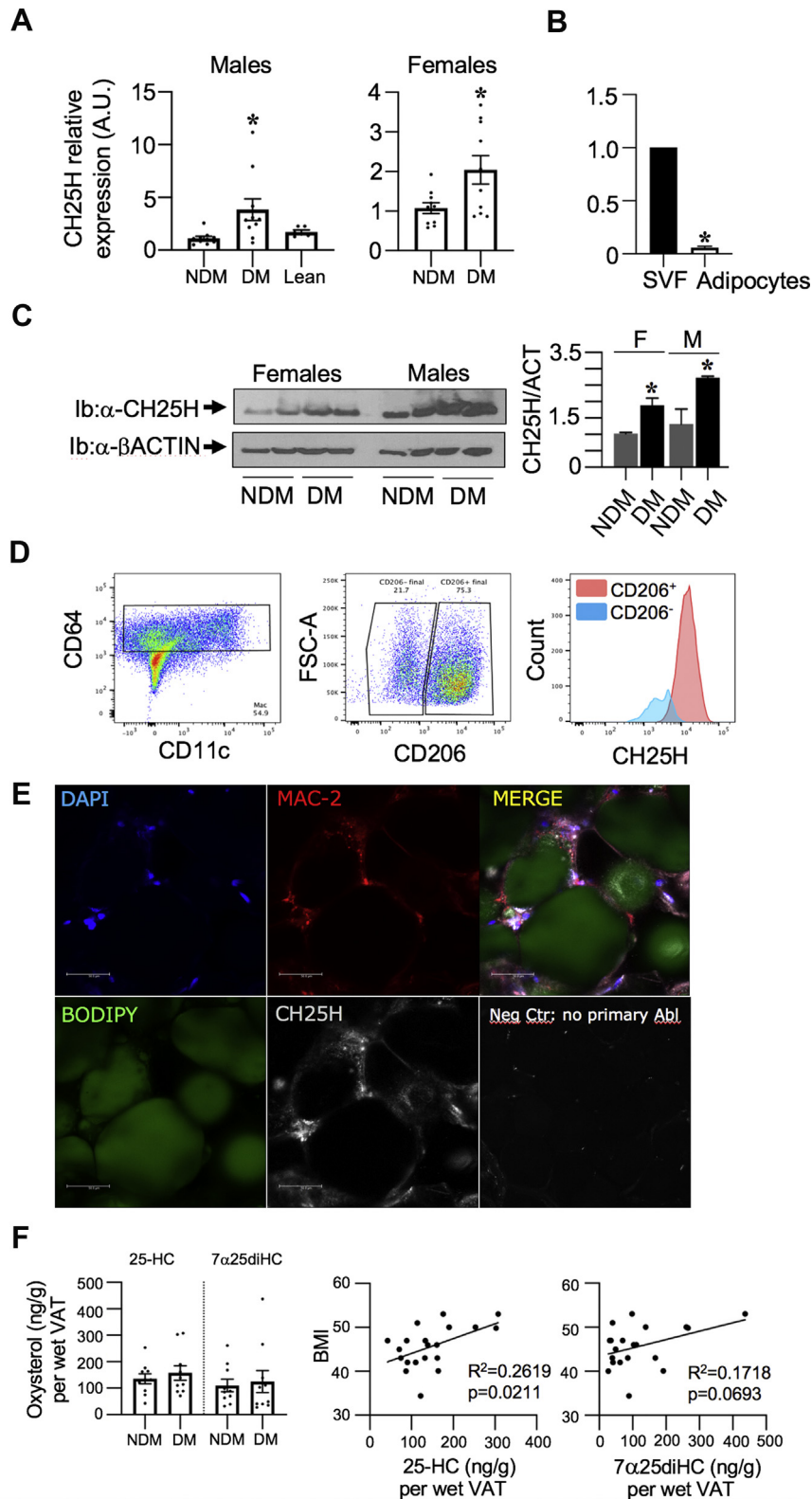


Figure 2: CH25H mRNA upregulation in human visceral omental adipose tissue of obese diabetic subjects and detection in ATMs. *A*) mRNA analysis of *CH25H* relative to *PPIA* in visceral omental adipose tissue (VAT) lysates from obese non-diabetic (NDM), obese diabetic (DM) and lean male subjects (N = 10 in duplicate and N = 6 lean in duplicate). Same assay in female subjects. *B*) The next to the upper graph shows CH25H expression in mature adipocytes and stromal vascular fraction (SVF) from omental fat. *C*) Western blot analysis of visceral omental adipose tissue lysates was performed to assess CH25H protein level (Ib: α-CH25H). The same gel was used to immunoblot with β-actin for normalization. Quantification of CH25H to Actin was measured by densitometry shown on the right. *D*) Flow cytometry blots show CD206⁺ cells out of CD64⁺CD11c⁺ ATMs and CH25H co-staining with CD206⁺ cells. *E*) Confocal microscopy in visceral omental adipose tissue sections of a representative obese diabetic male subject. Staining with DAPI/ nuclei (bleu), BODIPY/adipocytes (green), MAC-2/macrophages (red), Ch25h (grey) onto 20X field. Negative control was stained without primary antibody against CH25H but only with a fluorophore-conjugated secondary antibody. Values are expressed as mean ± SEM. *P ≤ 0.05 Significance compares to obese NDM. *F*) Levels of 25-HC and 7α25diHC in visceral omental adipose tissue from NDM and DM male subjects (N = 10). *G*) Correlational studies relative to age, BMI and HbA1c. Subject demographics in *ESM Table 3*.

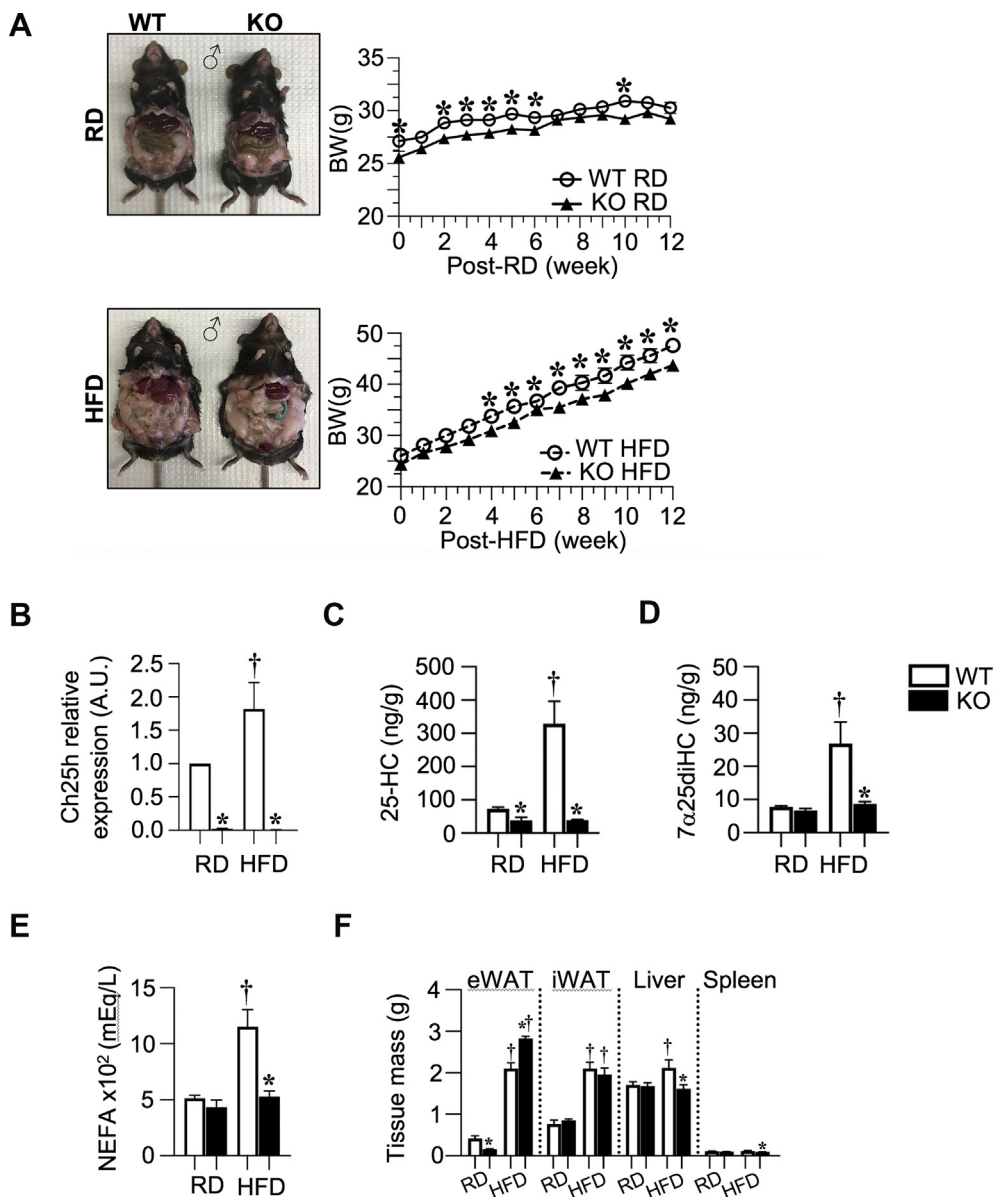


Figure 3: DIO-*Ch25h* knock-out mice are protected from BW gain and display increased adipose tissue mass. HFD induces *Ch25h* mRNA expression and 25-Hydroxycholesterol increase in mouse eWAT. A) Representative mice and BW curve in five-month-old *Ch25h* WT and KO mice fed a RD and HFD for 12 weeks starting at 9 weeks of age (N = 8/10 mice were used per each genotype and diet). B-D) The effect of high-fat diet was studied on the expression of *Ch25h* mRNA and the level of its produced oxysterol (25-HC) in epididymal white adipose tissue (eWAT) from RD and HFD fed *Ch25h* WT and KO (C57Bl/6j) male mice. QRT-PCR was conducted in duplicates (N = 5/group) and *Ch25h* expression was normalized to *Arbp1*. LC-MS/MS was conducted onto eWAT homogenates. 25-Hydroxycholesterol and 7α25dihydroxycholesterol were normalized by protein content of each homogenate and per total pad mass (N = 4/group). E) NEFA levels at fasting (o/n). F) Tissue mass (g). Values are expressed as mean ± SEM. **P* ≤ 0.05 *Ch25h* WT versus KO; †*P* ≤ 0.05 RD versus HFD/per each genotype.

3.4. *Ch25h* KO mice have augmented adipose tissue expandability and reduced inflammatory responses

To assess the metabolic consequences of *Ch25h* deletion, we measured plasma free fatty acids (NEFA) and noted no differences between WT and *Ch25h* KO mice on RD (Figure 3E). While NEFA levels increased with HFD in WT mice, NEFA levels were lower in HFD-fed *Ch25h* KO compared to *Ch25h* WT mice (Figure 3E). To examine hepatic steatosis, we assessed liver lipid content by histological analysis. No differences were seen in RD fed mice, but we observed a significant increase in lipid droplet deposition in HFD groups (Figure 4A). HFD-fed

Ch25h KO mice showed less lipid deposition in the liver compared to obese WT mice (Figure 4A) consistent with decreased liver mass (Figure 3F). NASH scoring supported a decrease in steatosis in *Ch25h* KO mice (Figure 4A). Despite an increase in the expression of main lipogenic genes (*Fasn*, *Ppara*) in response to HFD, no significantly different changes were measured between the two HFD-fed strains (ESM Fig. 6).

For adipose tissue, RD-fed *Ch25h* KO mice had smaller eWAT mass compared to lean *Ch25h* WT mice (Figure 3F). In contrast, HFD-fed *Ch25h* KO mice exhibited increased eWAT mass compared to obese

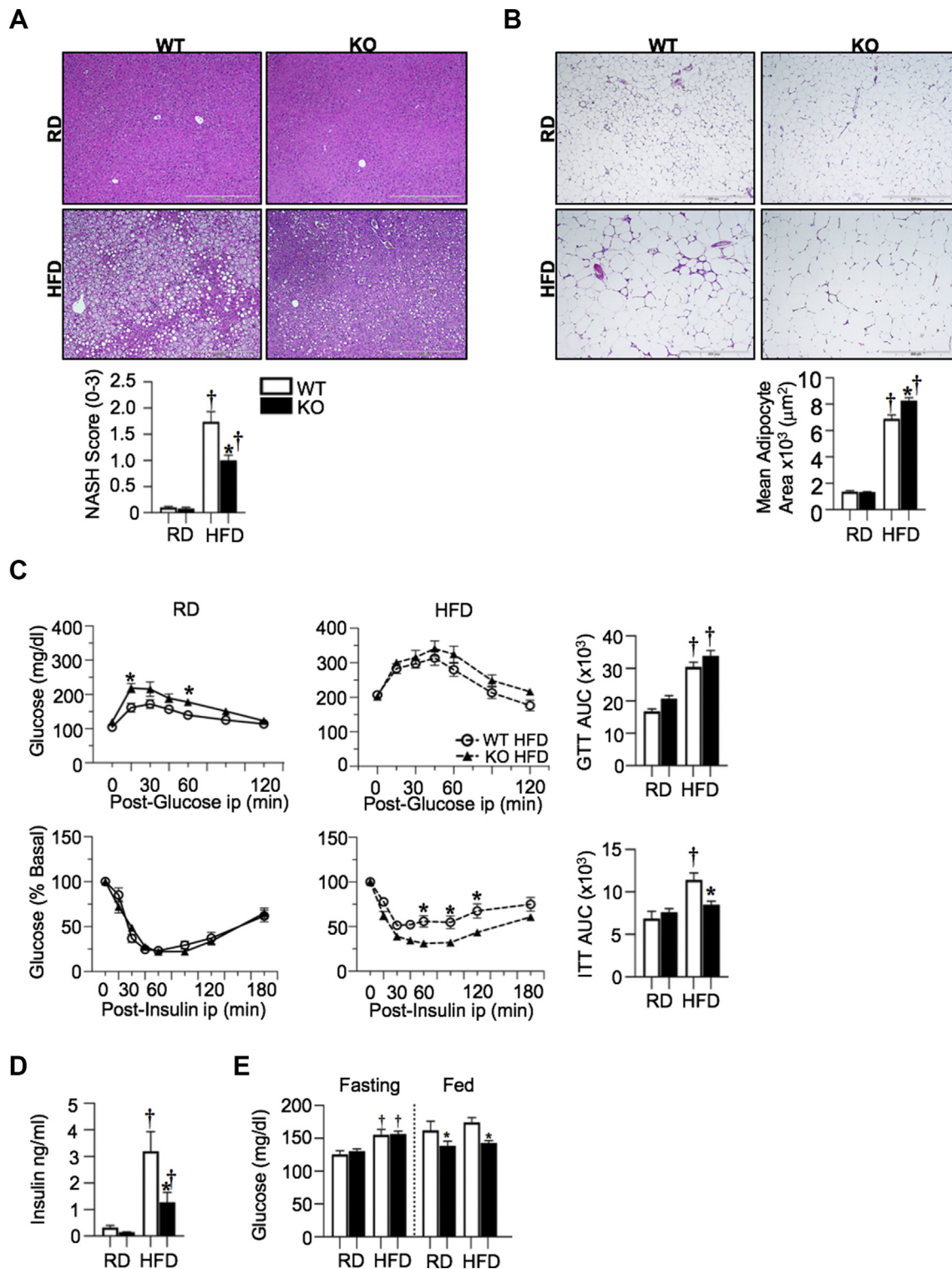


Figure 4: HFD-fed *Ch25h* knock-out mice display improved insulin action. *DIO-Ch25h* knock-out mice display less steatosis and increased adipose tissue expandability accompanied by less inflammatory gene expression. *A*) H&E stain in liver and NASH-score (N = 3/group). *B*) H&E stain in epididymal white adipose (N = 5/group). Images were collected onto a 10X field. Average adipocyte size was evaluated in the same samples. *C*) *In vivo* test for glucose clearance and insulin action post glucose and insulin ip injection (N = 8/10/group). AUC graphs are reported. *D*) Insulin levels at fasting (o/n). *E*) Glucose levels at fasting (6h) and fed state. Values are expressed as mean ± SEM. **P* ≤ 0.05 *Ch25h* WT versus KO; †*P* ≤ 0.05 RD versus HFD/per each genotype.

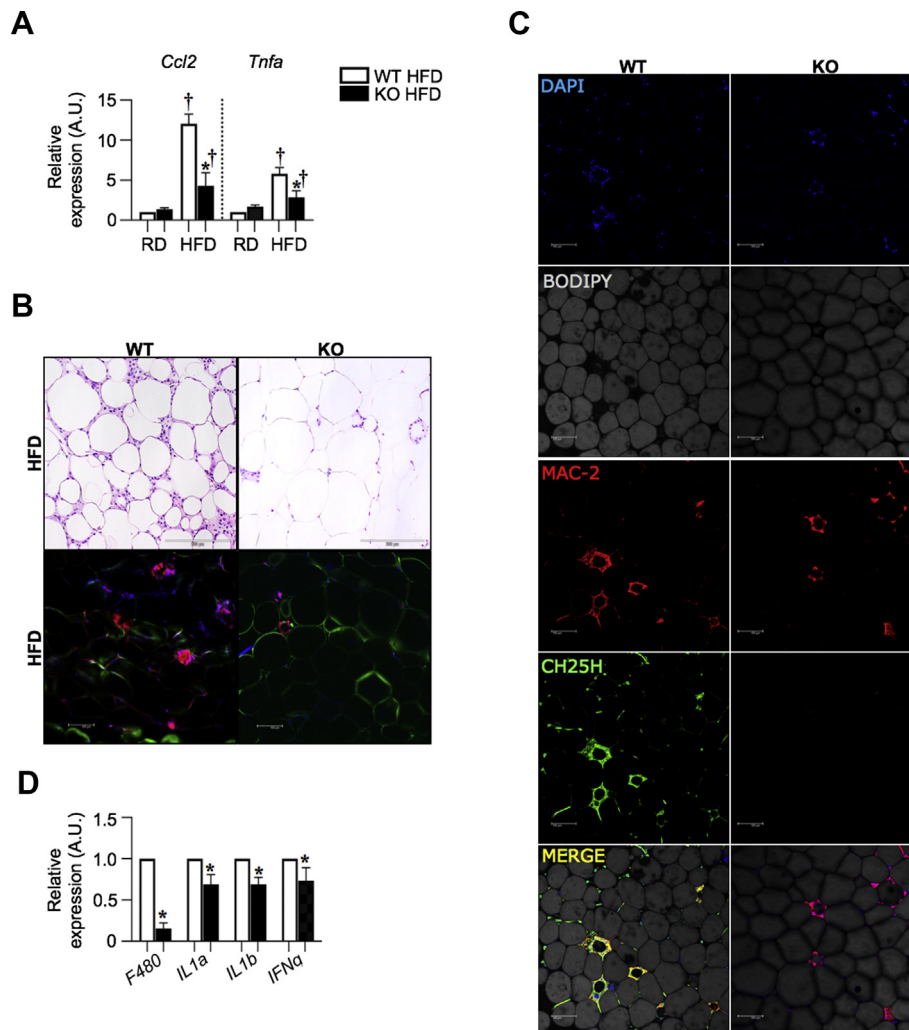


Figure 5: HFD-fed *Ch25h* knock-out mice display less ATM accumulation and inflammation in epididymal adipose tissue. A) QRT-PCR for mRNA expression of *Mcp1* and *Tnfa* genes in eWAT. Tissue were harvested at fed state. mRNA was analyzed in duplicate and normalized to *Arpb* (N = 5/group). B) H&E stain and confocal microscopy in epididymal white adipose tissue sections of representative *Ch25h* WT and KO male mice fed HFD showing less CLS formation in KO mice onto 20X field (N = 3/group). Staining with MAC-2/macrophages (red); DAPI/nuclei (bleu); Caveolin/adipocytes (green) onto 20X field (N = 3/group). C) Confocal microscopy in epididymal white adipose tissue sections of *Ch25h* WT and *Ch25h* KO male mice fed HFD (N = 3/group). Staining with DAPI/nuclei (bleu), BODIPY/adipocytes (grey), MAC-2/macrophages (red), Ch25h (green) onto a 20X field. D) Effect of *Ch25h* ablation on the mRNA expression of inflammatory genes in eWAT upon HFD. Tissue were harvested at fed state. mRNA was analyzed in duplicate and normalized to *Arpb* (N = 5/group). Values are expressed as mean \pm SEM. * $P \leq 0.05$ *Ch25h* WT versus KO.

Ch25h WT mice (Figure 3F), despite the slight decrease in total BW. Similar results were seen in three independent cohorts of mice including littermate controls (ESM Fig. 7A). Histologic analysis of eWAT showed similar morphology between WT and *Ch25h* KO RD fed mice (Figure 4B). In female mice, no differences were seen in tissue mass between WT and *Ch25h* KO (ESM Fig. 2C). eWAT of HFD-fed WT mice showed adipocyte hypertrophy and the presence of ATM-enriched, crown-like structures. In contrast, *Ch25h* KO mice showed fewer crown-like structures and had increased mean adipocyte size compared to obese *Ch25h* WT mice (Figure 4B). These data suggest that lack of *Ch25h* generates features of metabolically healthy obesity with decreased steatosis, increased adipocyte hypertrophy, and decreased circulating NEFA.

3.5. *Ch25h* is required for insulin resistance with HFD

To evaluate nutrient metabolism, we performed glucose tolerance tests (GTT) and insulin tolerance tests (ITT) in RD and HFD-fed mice

(Figure 4C). GTT in lean *Ch25h* KO mice showed mild glucose intolerance compared to WT mice without evidence of fasting hyperglycemia. Glucose metabolism was impaired in HFD groups compared to RD-fed mice and did not differ between genotypes. AUC confirmed these data (Figure 4C). However, when we conducted GTT test in WT and KO littermates, we observed improved glucose metabolism in obese KO mice compared to obese WT mice (ESM Fig. 7B). The insulin tolerance test did not show differences between RD groups (Figure 4C). When comparing RD versus HFD groups, both obese groups showed impaired insulin sensitivity based on ITT (Figure 4C). However, male *Ch25h* KO mice were more insulin sensitive compared to WT mice and supported by AUC. Consistently, we observed the same phenotype in male littermate mice (ESM Fig. 7B). Similar results were observed with HFD fed female mice (ESM Fig. 2B). Fasting insulin levels were higher in WT compared to *Ch25h* KO mice (Figure 4D). Glycemia at fasting and fed states were also collected. Fasting glycemia did not change between strains, unlike fed glycemia that was reduced in *Ch25h* KO

compared to WT, regardless of diet (Figure 3E). In females, differences in glycemia were not seen between the two strains (ESM Fig. 2D). Overall, this demonstrates that the lack of *Ch25h* is linked to altered insulin action in HFD-induced obesity.

3.6. Decreased inflammation in *Ch25h* KO mice

To assess metabolic inflammation in adipose tissue, we evaluated the expression of inflammatory genes in eWAT (Figure 5A). *Tnfa* and *Ccl2* mRNA expression in eWAT was significantly reduced in HFD *Ch25h* KO mice compared to controls (Figure 5A). No significant changes were seen between RD-fed strains (Figure 5A). H&E sections of eWAT of obese mice showed increased crown-like structure (CLS) formation in HFD-fed WT compared to *Ch25h* KO mice (Figure 5B). We also observed increased staining of MAC-2⁺ ATMs in WT obese mice compared to obese *Ch25h* KO mice (Figure 5B). Immunofluorescence staining verified the co-localization of Ch25h in macrophages in CLS (Figure 5C), similarly to what was observed in human VAT. In further support, the expression of inflammatory markers, such as F4/80, was significantly downregulated in *Ch25h* KO eWAT compared to WT (Figure 5D).

Next, we quantified adipose tissue leukocytes by flow cytometry (Figure 6). There were no significant differences in eWAT myeloid or lymphoid populations in RD-fed WT and *Ch25h* KO mice. HFD-fed KO mice had fewer total CD45⁺ leukocytes and CD11b⁺ myeloid cells compared to WT. CD64⁺CD11c⁺ ATMs and CD64⁺CD11c⁻ ATMs were not different between RD-fed WT and *Ch25h* KO mice. Consistent with the histology, there was a decrease of both CD11c⁺ and CD11c⁻ ATMs in eWAT of HFD-fed *Ch25h* KO compared to obese controls. Also, *Ch25h* KO mice had fewer CD64⁻CD11c⁺ adipose tissue dendritic cells compared to WT. Analysis of adipose tissue T cell content demonstrated fewer CD8⁺ T cells in eWAT of obese *Ch25h* KO mice compared to controls without significant differences in CD4⁺ T cells. Similar results were found in WT and KO littermates (ESM Fig. 7C). The

differences in leukocytes were specific to eWAT as no differences between genotypes were observed in sWAT and spleen of obese male mice (ESM Fig. 3A–B). No significant changes were found for T cells, monocytes, activated macrophages and neutrophils in the blood, except for less CD115⁺ Ly6C⁻ cells in *Ch25h* KO mice (ESM Fig. 3C). In HFD-fed *Ch25h* KO female mice, we found an increased number of CD3⁺ T cells and fewer CD115⁺ cells in KO than WT (ESM Fig. 2E). We did not observe significant differences of CD64⁺CD11c⁺ ATMs and CD64⁺CD11c⁻ ATMs in eWAT and sWAT between female WT and *Ch25h* KO mice (ESM Fig. 2F–G). In spleen CD64⁺CD11c⁺ ATMs and CD64⁻CD11c⁺ adipose tissue dendritic cells were lower in female *Ch25h* KO vs. WT (ESM Fig. 2H).

3.7. *Ch25h* is required for ATM activation to pro-inflammatory stimuli

To understand the mechanisms by which *Ch25h* may contribute to metabolic inflammation, we evaluated BMDMs from WT and *Ch25h* KO mice. *Nos2* induction was attenuated in LPS-primed BMDMs from *Ch25h* KO compared to WT (Figure 7A). Treatment of BMDMs with TNFα did not induce *Nos2*, and the co-treatment of BMDMs with LPS and TNFα led to lower *Nos2* induction in *Ch25h* KO mice. Similar results were seen for the *Ccl2* expression level in response to stimuli (Figure 7A). To assess if these attenuated inflammatory responses were relevant in adipose tissue, we exposed eWAT explants from lean male mice to LPS or LPS + TNFα ex vivo (Figure 7B). LPS induced *Nos2*, *Ccl2* and *Il6* gene expression in WT explants, but these effects were significantly attenuated in *Ch25h* KO eWAT explants. In contrast, while *Il1b* was induced by LPS in explants, this was not dependent on *Ch25h*. *Ch25h*-dependent *Nos2* and *Il6* induction was also observed in explants treated with both LPS and TNFα. TNFα alone did not significantly increase *Nos2* or *Il6*. *Ccl2* and *Il6* were induced in response to TNFα alone, but no changes were seen between WT and *Ch25h* KO eWAT explants. However, the induction of *Nos2* and *Ccl2* were

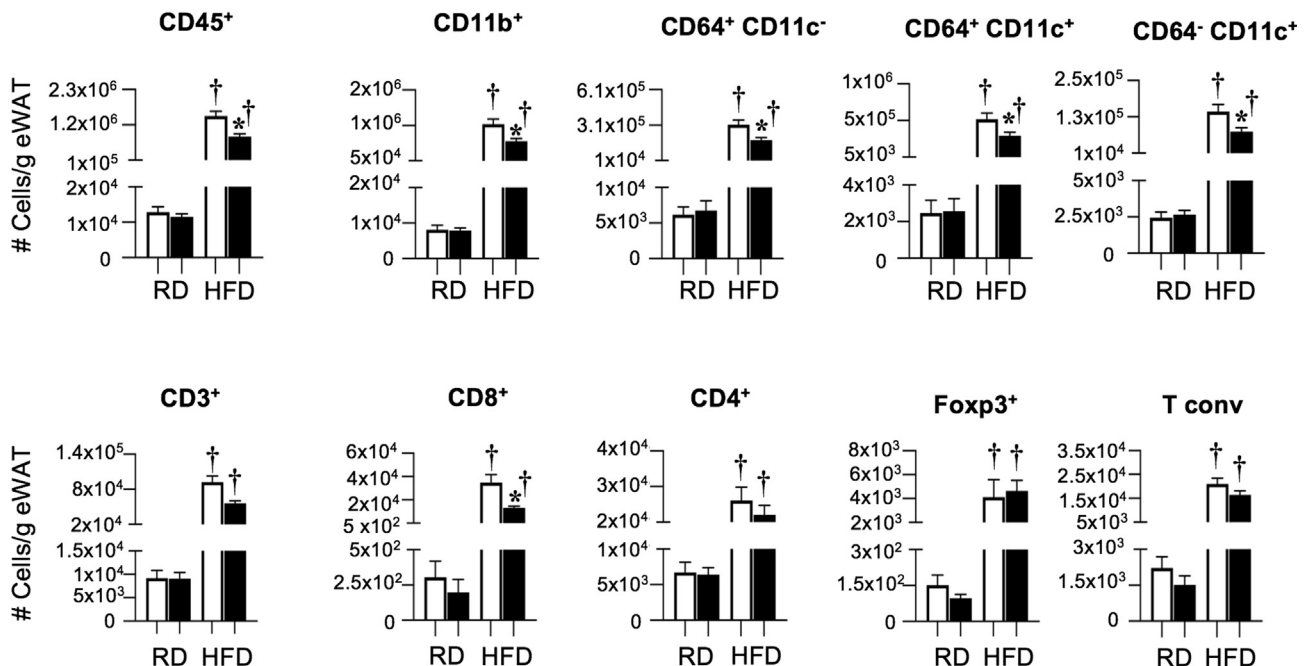


Figure 6: Immunologic profiling in *Ch25h* knock-out mice displays decreased pro-inflammatory ATMs and CD8⁺ T cells in eWAT. Stromal vascular fraction (SVF) from epididymal white adipose tissue of obese *Ch25h* WT and KO male mice was analyzed by FACS (N = 8–10/group). FACS plot data of ATM populations and CD4⁺, CD8⁺ T cells are shown. Cell number was normalized to total tissue mass.

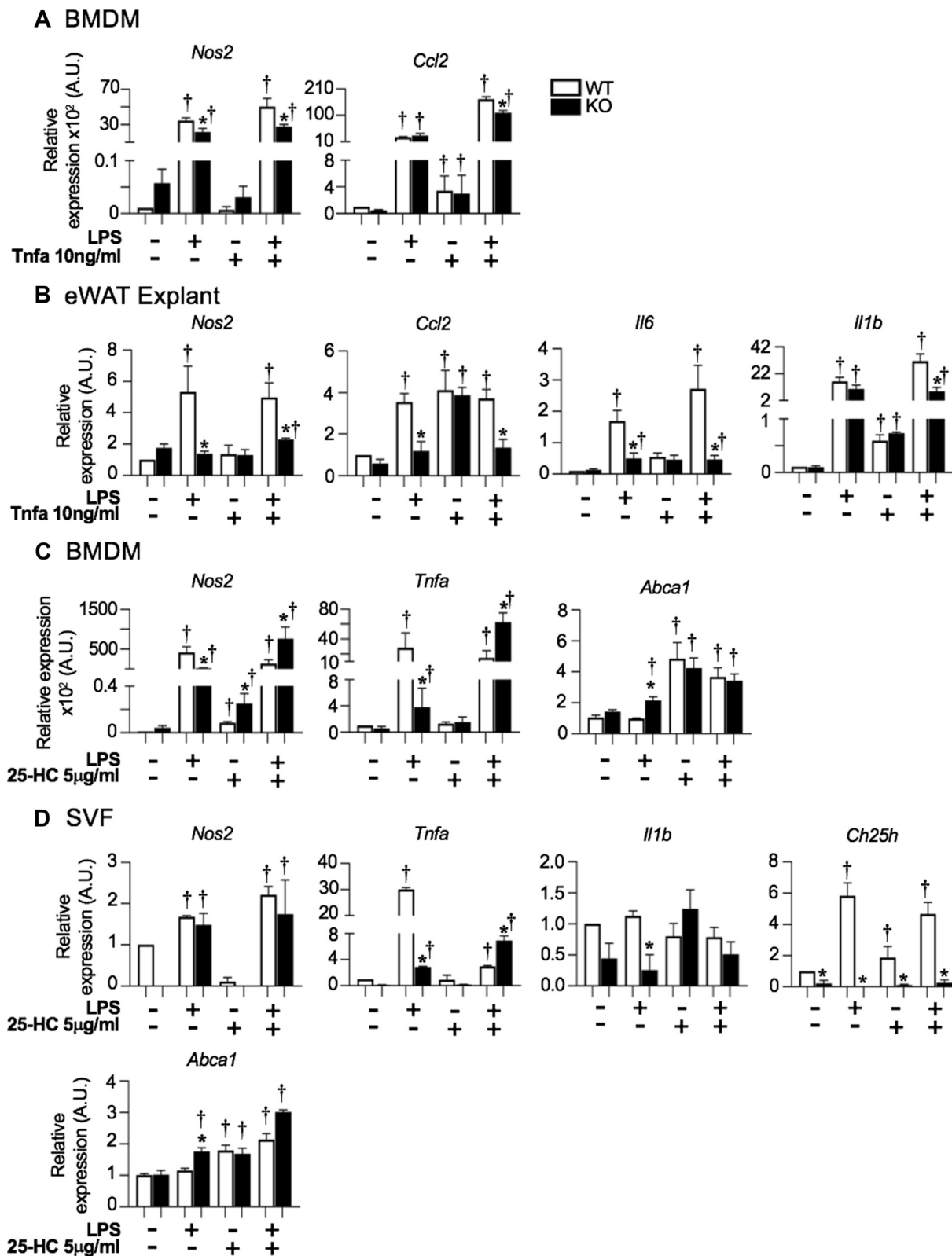
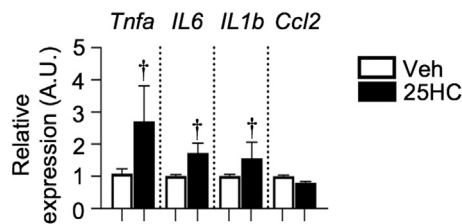


Figure 7: Effect of LPS-Tn α and 25-HC on the mRNA levels of inflammatory genes in BMDMs, eWAT explants and SVF cells from *Ch25h* wild-types and knock-outs. Effect of LPS and Tn α on the mRNA expression of inflammatory genes in A) BMDMs, and B) eWAT explants. Effect of 25-Hydroxycholesterol on the mRNA expression of inflammatory genes in C) BMDMs, D) eWAT-derived SVF cells. BMDMs, SVF of eWAT were obtained from 4-month-old RD fed *Ch25h* WT and KO male mice. Cells and tissues were treated with either vehicle alone (Veh) or with lipopolysaccharide (LPS 100 ng/ml for 8 h) or with tumor necrosis factor alpha (Tn α 10 ng/ml for 8 h) alone or in combination (n = 3 wells/genotype/treatment). In the other experiment, 25-Hydroxycholesterol (25-HC 5 μ g/ml for 8 h) was added with/without LPS in replacement of Tn α . mRNA was analyzed in duplicate and normalized to *Arpb*. Values are expressed as mean \pm SEM. †*P* < 0.05 treatment versus Veh; **P* \leq 0.05 *Ch25h* WT versus KO.

A 3T3-L1 Cells



B Human pre-adipocytes

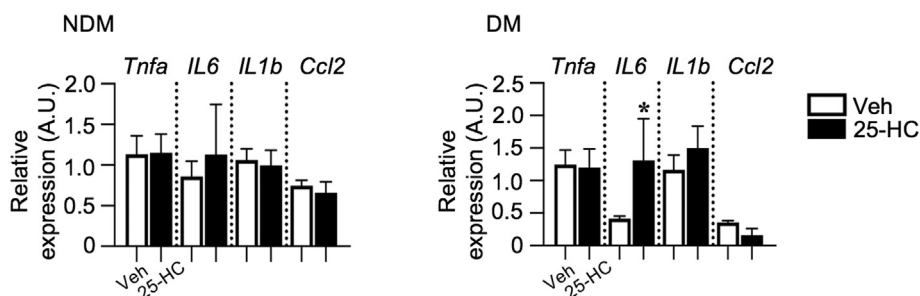


Figure 8: Effect of 25-HC on the mRNA levels of inflammatory genes in murine and human pre-adipocytes. A) 3T3-L1 cells and B) human pre-adipocytes from VAT of NDM and DM subjects. Not differentiated cells were treated with either vehicle alone (Veh) or with 25-Hydroxycholesterol (25-HC 5 μ g/ml for 8 h). mRNA was analyzed in duplicate and normalized to *PPIA*. Values are expressed as mean \pm SEM. * $P < 0.05$ treatment versus Veh.

attenuated with co-exposure of eWAT to LPS and TNF α . Moreover, *Il1b* was reduced in *Ch25h* KO explants compared to WT with co-treatment with LPS and TNF α . This suggests that *Ch25h* KO ATMs fail to activate with classical pro-inflammatory stimuli with LPS.

To address whether the Ch25h requirement for inflammatory activation was directly mediated by 25-HC, we treated BMDMs (Figure 7C) and eWAT SVF cells (Figure 7D) from WT and *Ch25h* KO mice with 25-HC. As seen previously, *Ch25h* KO BMDMs had decreased *Nos2* and *Tnfa* expression in response to LPS compared to WT. 25-HC addition to WT BMDMs increased *Nos2*, but not *Tnfa* expression, in both strains compared to untreated cells. The addition of 25-HC was sufficient to reconstitute *Nos2* and *Tnfa* gene expression in LPS stimulated *Ch25h* KO BMDMs (Figure 7C). This suggests that 25-HC is sufficient to restore inflammatory responses in the absence of Ch25h.

To examine the effect of 25-HC in adipose, we examined cultured SVF cells from lean eWAT. Stimulation of WT eWAT SVF cells with LPS led to an induction of *Nos2* and *Tnfa* (Figure 7D). In response to LPS alone and LPS+25-HC, the induction of *Nos2* was seen in both strains to a similar extent. *Tnfa* expression was significantly lower in *Ch25h* KO SVF cells compared to WT following LPS treatment. *Tnfa* expression was not altered by the addition of 25-HC alone. Importantly, 25-HC partially restored the induction of *Tnfa* in response to LPS consistent with the requirement for 25-HC and CH25H in generating maximal inflammatory responses in adipose tissue. *Il1b* was also measured, but no relevant changes were seen, given that in response to LPS, no induction was observed. *Ch25h* gene expression was used as a control. LPS induced *Ch25h* expression alone and in combination with 25-HC. 25-HC increases *Ch25h* expression itself. Given that 25-HC is an LXR agonist [38], we measured the expression of the LXR dependent gene *Abca1* in BMDMs (Figure 7C) and SVF cells (Figure 7D). *Abca1* was significantly elevated in response to 25-HC, suggesting an LXR-dependent mechanism of induced expression.

3.8. 25-HC promotes the expression of pro-inflammatory genes in preadipocytes

To examine the contribution of CH25H on other components in adipose tissue, we assessed the effect of 25-HC on 3T3-L1 cells and primary human preadipocytes from omental VAT from obese patients. In response to 25-HC, we observed the induction of *Tnfa*, *Il6*, *Il1b* expression in 3T3-L1 preadipocytes (Figure 8A). *IL6* gene expression was induced in human preadipocytes from patients with DM, but not in those without DM (Figure 8B). This suggests that macrophage derived 25-HC can induce inflammatory gene expression in preadipocytes in a diabetes specific manner.

4. DISCUSSION

This study advances our understanding of how the 25-HC producing enzyme, CH25H, contributes to obesity-induced inflammation. Our study highlights several primary observations: 1) we observed a positive association between CH25H upregulation in AT and obesity/DM status; 2) *Ch25h* is required for HFD-induced insulin resistance and adipose tissue inflammation in mice; 3) ATMs are the primary site of CH25H expression in humans and mice and is induced with inflammatory stimuli; and 4) 25-HC is sufficient to induce inflammatory gene expression in macrophages and preadipocytes from DM subjects. Our interest in CH25H extended from the observation that *CH25H* is increased in VAT of obese DM subjects compared to obese subjects without diabetes suggesting a mechanistic role for CH25H in insulin resistance. Our finding agrees with data showing that CH25H is downregulated in adipose tissue of obese subjects after bariatric surgery [19]. Consistent with reports of Ch25h expression in myeloid cells [39], we observed that CH25H is expressed in human and murine ATMs, specifically, CD206⁺ ATMs in human VAT, a subpopulation that has been suggested to be associated with insulin resistance [40]. Consistently, with a pro-inflammatory role, we observed that *Ch25h* is

an HFD-induced gene and its overexpression occurs in mouse visceral adipose tissue.

HFD-induced 25-HC and 7 α 25diHC in visceral adipose tissue in mice is dependent on *Ch25h*. A previous study showed decreased levels of 25-HC in subcutaneous adipose tissue and liver of DIO mice [41]. Conversely, in the liver of *db/db* and *ob/ob* mice, this study reported increased levels of 25-HC in subcutaneous adipose tissue, but this was not accompanied by an increase in *Ch25h* expression [41]. Increased levels of 25-HC and 7 α 25diHC, accompanied by increased mRNA expression of *Ch25h*, were also found in mice with acute colon inflammation. Data were confirmed in the inflamed colon of patients with ulcerative colitis [42]. Lack of data regarding 25-HC levels in visceral adipose tissue of DM subjects led us to measure the concentration of this oxysterol and 7 α 25diHC in human VAT where we observed a correlation between 25-HC and BMI in this obese population. In our cohort of VAT samples, 25-HC and 7 α 25diHC, were detected in the range of 42.4–308 ng/g and 27.4–437 ng/g, respectively. However, we didn't observe significant differences between obese NDM and DM subjects. This may be due to our relatively small cohort size or due to regional differences in 25-HC production.

Global deletion of *Ch25h* led to improved hyperinsulinemia, insulin sensitivity, steatosis, and adipose tissue health compared to obese WT mice. Mechanistically, we feel that less ectopic lipid deposit in the liver was due to improved adipose tissue lipid storage due to less inflammation. However, as an independent and alternative mechanism, reduced liver steatosis could also be linked to the regulation of 25-HC on *Insig1* [43] and its implication in *de novo* lipogenesis [44]. The improvement in adipose tissue health and expandability in obese *Ch25h* KO mice was due to a reduction of CD11c⁺ ATM accumulation and activation, and from the decrease in inflammatory cytokine expression. Notably, the lower number of CD8⁺ T cells might also have exerted a role in lowering the recruitment and activation of ATMs in *Ch25h* KO mice, and this could have explained the decreased accumulation of ATMs. While 25-HC was reported to control the differentiation of monocytes into macrophages [45], we did not observe any significant change in the number of CD115⁺ Ly6C⁺ monocytes but fewer CD115⁺ Ly6C⁻ monocytes in obese *Ch25h* KO mice compared to obese WT mice. Thus based on a potential transition of these cells, we could also consider this latter mechanism related to less circulating monocytes as a causative phenomenon of decreased recruitment of ATMs in adipose tissue.

The literature supports both pro- and anti-inflammatory roles for 25-HC dependent on the experimental model, the stimulus used, as well as the cell type studied. Our *in vitro* studies, demonstrated that in the absence of Ch25h/25-HC, macrophages failed to undergo a substantial activation upon inflammatory stimuli. This was seen in BMDMs and more strongly proved by lower expression level of *NOS2*, *Ccl2*, *IL6*, *IL1 β* genes in eWAT explants treated with LPS and TNFa. These explants represented a direct source of ATMs in their environment. Although in a different model of murine influenza infection, our data confirmed a previous observation that reported IL6 production by macrophages in response to 25-HC [21]. Its effect appeared to be mediated by the recruitment of AP-1 components FOS and Jun to promote a subset of TLR responsive genes [21]. In support of our findings, additional published data demonstrated that 25-HC amplified the secretion of inflammatory cytokines, such as macrophage colony-stimulating factor (M-CSF), IL6, and IL8 [46,47].

Furthermore, Ch25h/25-HC played a role in the negative feedback mechanism that regulates the production of IL1 family cytokines during

inflammatory processes in response to the stimulation with type I IFN [48]. 25-HC had a repressive effect on IL1b expression and acted as a broad inhibitor of inflammasome activity. Conversely, it was shown that 25-HC increased IL1b mRNA expression and secretion following LPS challenge in human monocyte-derived macrophages [49]. Our data remained in line with this latter observation, suggesting 25-HC as an inducer of IL1b in an obesogenic environment.

Finally, the literature provided conflictual data concerning the implication of 25-HC on the regulation of Tnfa expression. According to one study, 25-HC reduced LPS-induced macrophage Tnfa expression and secretion [50]. Conversely, we observed the induction of Tnfa expression in BMDMs and eWAT-SVF cells treated with 25-HC. Further investigation will be critical to address the mechanisms by which 25-HC regulates the expression of pro-inflammatory cytokines, such as Tnfa, in the obese setting. Given that from previous work, 25-HC was shown to induce the expression of pro-inflammatory cytokines via ERK1/2 and JNK phosphorylation of FOS and JUN, and NF- κ B activation [51,52], we will also pursue this road of investigation as one of our future goals.

5. CONCLUSIONS

We demonstrate an association between CH25H expression and DM status in obese patients as well as a positive correlation of 25-HC in VAT with BMI. We proved that Ch25h is an HFD-induced gene and, as a result, HFD increased the concentration of 25-HC in AT. Based on the finding that the whole-body ablation of Ch25h might protect obese mice from meta-inflammation and ameliorate insulin resistance, we propose that CH25H/25-HC could have a detrimental effect on the regulation of AT-inflammation. Additionally, we assigned a pro-inflammatory role to 25-HC, given to its effect on the expression of pro-inflammatory cytokines, such as Tnfa. Finally, we believed that our data, obtained using parallel and complementary approaches between human and murine systems, could have the potential to contribute to new “translatable” knowledge regarding the role of Ch25h/25-HC in the development of meta-inflammation and associated insulin resistance.

AUTHOR CONTRIBUTION

L.R. contributed to experimental design and performed all experiments except RNASeq analysis and oxysterol measure. She contributed to data interpretation and wrote the manuscript.

L.M. and L.G. performed RNASeq analysis.

J.D.P. contributed to mouse profiling.

N.B. and C.F. contributed to human adipose tissue biopsy collection.

R.O.R. contributed to human samples and dataset collection.

C.N.L. contributed to experimental design, data interpretation, and manuscript writing.

FINANCIAL SUPPORT

This work was supported by a grant of Dr. Carey N. Lumeng. The funding source of Dr. Lumeng: NIH R01 DK090262 and DK115190. University of Michigan Medical School and the Department of Pediatrics and Pulmonary Medicine and the Department of Surgery.

CONFLICT OF INTEREST

The authors declare no conflict of interest associated with this manuscript.

APPENDIX A. SUPPLEMENTARY DATA

Supplementary data to this article can be found online at <https://doi.org/10.1016/j.molmet.2020.100983>.

REFERENCES

- [1] Nguyen, D.M., El-Serag, H.B., 2010. The epidemiology of obesity. *Gastroenterology Clinics of North America* 39(1):1–7. <https://doi.org/10.1016/j.gtc.2009.12.014>. PubMed PMID: 20202574; PMCID: PMC2833287.
- [2] Maffetone, P.B., Rivera-Dominguez, I., Laursen, P.B., 2016. Overfat and underfat: new terms and definitions long overdue. *Front Public Health* 4:279. <https://doi.org/10.3389/fpubh.2016.00279>. PubMed PMID: 28097119; PMCID: PMC5206235.
- [3] Bluher, S., Schwarz, P., 2014. Metabolically healthy obesity from childhood to adulthood - does weight status alone matter? *Metabolism* 63(9):1084–1092. <https://doi.org/10.1016/j.metabol.2014.06.009>. PubMed PMID: 25038727.
- [4] Guilherme, A., Virbasius, J.V., Puri, V., Czech, M.P., 2008. Adipocyte dysfunctions linking obesity to insulin resistance and type 2 diabetes. *Nature Reviews Molecular Cell Biology* 9(5):367–377. <https://doi.org/10.1038/nrm2391>. PubMed PMID: 18401346; PMCID: PMC2886982.
- [5] Kim, J.B., 2016. Dynamic cross talk between metabolic organs in obesity and metabolic diseases. *Experimental & Molecular Medicine* 48:e214. <https://doi.org/10.1038/emm.2015.119>. PubMed PMID: 26964830; PMCID: PMC4892875.
- [6] Saltiel, A.R., Olefsky, J.M., 2017. Inflammatory mechanisms linking obesity and metabolic disease. *Journal of Clinical Investigation* vol. 127(1):1–4. <https://doi.org/10.1172/JCI92035>. PubMed PMID: 28045402; PMCID: PMC5199709 treatment of metabolic disease. J.M. Olefsky owns stock in Catabasis Pharmaceuticals and receives consulting income from Cymabay Inc., Second Genome, and AntriaBio.
- [7] Stefan, N., Haring, H.U., Hu, F.B., Schulze, M.B., 2013. Metabolically healthy obesity: epidemiology, mechanisms, and clinical implications. *Lancet Diabetes Endocrinol* 1(2):152–162. [https://doi.org/10.1016/S2213-8587\(13\)70062-7](https://doi.org/10.1016/S2213-8587(13)70062-7). PubMed PMID: 24622321.
- [8] Kratz, M., Coats, B.R., Hisert, K.B., Hagman, D., Mutskov, V., Peris, E., et al., 2014. Metabolic dysfunction drives a mechanistically distinct proinflammatory phenotype in adipose tissue macrophages. *Cell Metabolism* 20(4):614–625. <https://doi.org/10.1016/j.cmet.2014.08.010>. PubMed PMID: 25242226; PMCID: PMC4192131.
- [9] Xu, X., Grijalva, A., Skowronski, A., van Eijk, M., Serlie, M.J., Ferrante Jr., A.W., 2013. Obesity activates a program of lysosomal-dependent lipid metabolism in adipose tissue macrophages independently of classic activation. *Cell Metabolism* 18(6):816–830. <https://doi.org/10.1016/j.cmet.2013.11.001>. PubMed PMID: 24315368; PMCID: PMC3939841.
- [10] Pecht, T., Haim, Y., Bashan, N., Shapiro, H., Harman-Boehm, I., Kirshtein, B., et al., 2016. Circulating blood monocyte subclasses and lipid-laden adipose tissue macrophages in human obesity. *PLoS One* 11(7):e0159350. <https://doi.org/10.1371/journal.pone.0159350>. PubMed PMID: 27442250; PMCID: PMC4956051.
- [11] Chawla, A., Nguyen, K.D., Goh, Y.P., 2011. Macrophage-mediated inflammation in metabolic disease. *Epub 2011/10/11 Nature Reviews Immunology* 11(11):738–749. <https://doi.org/10.1038/nri3071>. PubMed PMID: 21984069; PMCID: PMC3383854.
- [12] Makki, K., Froguel, P., Wolowczuk, I., 2013. Adipose tissue in obesity-related inflammation and insulin resistance: cells, cytokines, and chemokines. *ISRN Inflammation* 2013:139239. <https://doi.org/10.1155/2013/139239>. PubMed PMID: 24455420; PMCID: PMC3881510.
- [13] Bertola, A., Ciucci, T., Rousseau, D., Bourlier, V., Duffaut, C., Bonnafous, S., et al., 2012. Identification of adipose tissue dendritic cells correlated with obesity-associated insulin-resistance and inducing Th17 responses in mice and patients. *Diabetes* 61(9):2238–2247. <https://doi.org/10.2337/db11-1274>. PubMed PMID: 22596049; PMCID: PMC3425417.
- [14] Morris, D.L., Cho, K.W., DelProposto, J.L., Oatman, K.E., Geletka, L.M., Martinez-Santibanez, G., et al., 2013. Adipose tissue macrophages function as antigen-presenting cells and regulate adipose tissue CD4+ T cells in mice. *Diabetes* 62(8):2762–2772. <https://doi.org/10.2337/db12-1404>. PubMed PMID: 23493569; PMCID: PMC3717880.
- [15] Cho, K.W., Morris, D.L., DelProposto, J.L., Geletka, L., Zamarron, B., Martinez-Santibanez, G., et al., 2014. An MHC II-dependent activation loop between adipose tissue macrophages and CD4+ T cells controls obesity-induced inflammation. *Cell Reports* 9(2):605–617. <https://doi.org/10.1016/j.celrep.2014.09.004>. PubMed PMID: 25310975; PMCID: PMC4252867.
- [16] Russo, L., Lumeng, C.N., 2018. Properties and functions of adipose tissue macrophages in obesity. *Immunology*. <https://doi.org/10.1111/imm.13002>. PubMed PMID: 30229891.
- [17] Li, Z., Martin, M., Zhang, J., Huang, H.Y., Bai, L., Zhang, J., et al., 2017. KLF4 regulation of Ch25h and LXR mitigates atherosclerosis susceptibility. *Circulation*. <https://doi.org/10.1161/CIRCULATIONAHA.117.027462>. PubMed PMID: 28794002.
- [18] Chen, Y., Zhu, J., Lum, P.Y., Yang, X., Pinto, S., MacNeil, D.J., et al., 2008. Variations in DNA elucidate molecular networks that cause disease. *Nature* 452(7186):429–435. Epub 2008/03/18. doi: nature06757 [pii] 10.1038/nature06757. PubMed PMID: 18344982.
- [19] Dankel, S.N., Fadnes, D.J., Stavrum, A.K., Stansberg, C., Holdhus, R., Hoang, T., et al., 2010. Switch from stress response to homeobox transcription factors in adipose tissue after profound fat loss. *PLoS One* 5(6):e11033. <https://doi.org/10.1371/journal.pone.0011033>. PubMed PMID: 20543949; PMCID: PMC2882947.
- [20] Diczfalusy, U., Olofsson, K.E., Carlsson, A.M., Gong, M., Golenbock, D.T., Rooyackers, O., et al., 2009. Marked upregulation of cholesterol 25-hydroxylase expression by lipopolysaccharide. *The Journal of Lipid Research* 50(11):2258–2264. <https://doi.org/10.1194/jlr.M900107-JLR200>. PubMed PMID: 19502589; PMCID: PMC2759831.
- [21] Gold, E.S., Diercks, A.H., Podolsky, I., Podyminogin, R.L., Askovich, P.S., Treuting, P.M., et al., 2014. 25-Hydroxycholesterol acts as an amplifier of inflammatory signaling. *Proceedings of the National Academy of Sciences of the United States of America* 111(29):10666–10671. <https://doi.org/10.1073/pnas.1404271111>. PubMed PMID: 24994901; PMCID: PMC4115544.
- [22] Liu, S.Y., Aliyari, R., Chikere, K., Li, G., Marsden, M.D., Smith, J.K., et al., 2013. Interferon-inducible cholesterol-25-hydroxylase broadly inhibits viral entry by production of 25-hydroxycholesterol. *Immunity* 38(1):92–105. <https://doi.org/10.1016/j.immuni.2012.11.005>. PubMed PMID: 23273844; PMCID: PMC3698975.
- [23] Song, Z., Zhang, Q., Liu, X., Bai, J., Zhao, Y., Wang, X., et al., 2017. Cholesterol 25-hydroxylase is an interferon-inducible factor that protects against porcine reproductive and respiratory syndrome virus infection. *Veterinary Microbiology* 210:153–161. <https://doi.org/10.1016/j.vetmic.2017.09.011>. PubMed PMID: 29103685.
- [24] Liu, Y., Wei, Z., Ma, X., Yang, X., Chen, Y., Sun, L., et al., 2018. 25-Hydroxycholesterol activates the expression of cholesterol 25-hydroxylase in an LXR-dependent mechanism. *The Journal of Lipid Research* 59(3):439–451. <https://doi.org/10.1194/jlr.M080440>. PubMed PMID: 29298812; PMCID: PMC5832929.
- [25] Bauman, D.R., Bitmansour, A.D., McDonald, J.G., Thompson, B.M., Liang, G., Russell, D.W., 2009. 25-Hydroxycholesterol secreted by macrophages in response to Toll-like receptor activation suppresses immunoglobulin A production. *Proceedings of the National Academy of Sciences of the United States of America* 106(39):16764–16769. <https://doi.org/10.1073/pnas.0909142106>. PubMed PMID: 19805370; PMCID: PMC2757821.

- [26] Li, C., Deng, Y.Q., Wang, S., Ma, F., Aliyari, R., Huang, X.Y., et al., 2017. 25-Hydroxycholesterol protects host against zika virus infection and its associated microcephaly in a mouse model. *Immunity* 46(3):446–456. <https://doi.org/10.1016/j.immuni.2017.02.012>. PubMed PMID: 28314593; PMCID: PMC5957489.
- [27] Noebauer, B., Jais, A., Todoric, J., Gossens, K., Sutterluty-Fall, H., Einwallner, E., 2017. Hepatic cholesterol-25-hydroxylase overexpression improves systemic insulin sensitivity in mice. *Journal of Diabetes Research* 2017: 4108768. <https://doi.org/10.1155/2017/4108768>. PubMed PMID: 28299341; PMCID: PMC5337352.
- [28] Tuong, Z.K., Lau, P., Yeo, J.C., Pearen, M.A., Wall, A.A., Stanley, A.C., et al., 2013. Disruption of Roralpha1 and cholesterol 25-hydroxylase expression attenuates phagocytosis in male Roralphasg mice. *Endocrinology* 154(1): 140–149. <https://doi.org/10.1210/en.2012-1889>. PubMed PMID: 23239817.
- [29] Tuong, Z.K., Lau, P., Du, X., Condon, N.D., Goode, J.M., Oh, T.G., et al., 2016. RORalpha and 25-hydroxycholesterol crosstalk regulates lipid droplet homeostasis in macrophages. *PLoS One* 11(1):e0147179. <https://doi.org/10.1371/journal.pone.0147179>. PubMed PMID: 26812621; PMCID: PMC4727927.
- [30] Choi, W.S., Lee, G., Song, W.H., Koh, J.T., Yang, J., Kwak, J.S., et al., 2019. The CH25H-CYP7B1-RORalpha axis of cholesterol metabolism regulates osteoarthritis. *Nature* 566(7743):254–258. <https://doi.org/10.1038/s41586-019-0920-1>. PubMed PMID: 30728500.
- [31] Cho, K.W., Zamarron, B.F., Muir, L.A., Singer, K., Porsche, C.E., DelProposto, J.B., et al., 2016. Adipose tissue dendritic cells are independent contributors to obesity-induced inflammation and insulin resistance. *The Journal of Immunology* 197(9):3650–3661. <https://doi.org/10.4049/jimmunol.1600820>. PubMed PMID: 27683748.
- [32] Zamarron, B.F., Mergian, T.A., Cho, K.W., Martinez-Santibanez, G., Luan, D., Singer, K., et al., 2017. Macrophage proliferation sustains adipose tissue inflammation in formerly obese mice. *Diabetes* 66(2):392–406. <https://doi.org/10.2337/db16-0500>. PubMed PMID: 28108608; PMCID: PMC5248991.
- [33] Martinez-Santibanez, G., Cho, K.W., Lumeng, C.N., 2014. Imaging white adipose tissue with confocal microscopy. *Methods in Enzymology* 537:17–30. <https://doi.org/10.1016/B978-0-12-411619-1.00002-1>. PubMed PMID: 24480339; PMCID: PMC4233125.
- [34] Muir, L.A., Neeley, C.K., Meyer, K.A., Baker, N.A., Brosius, A.M., Washabaugh, A.R., et al., 2016. Adipose tissue fibrosis, hypertrophy, and hyperplasia: correlations with diabetes in human obesity. *Obesity* 24(3):597–605. <https://doi.org/10.1002/oby.21377>. PubMed PMID: 26916240; PMCID: PMC4920141.
- [35] Cho, K.W., Morris, D.L., Lumeng, C.N., 2014. Flow cytometry analyses of adipose tissue macrophages. *Methods in Enzymology* 537:297–314. <https://doi.org/10.1016/B978-0-12-411619-1.00016-1>. PubMed PMID: 24480353; PMCID: PMC4244227.
- [36] Muir, L.A., Kiridena, S., Griffin, C., DelProposto, J.B., Geletka, L., Martinez-Santibanez, G., et al., 2018. Frontline Science: rapid adipose tissue expansion triggers unique proliferation and lipid accumulation profiles in adipose tissue macrophages. *Journal of Leukocyte Biology* 103(4):615–628. <https://doi.org/10.1002/JLB.3HI1017-422R>. PubMed PMID: 29493813.
- [37] Russo, L., Ghadieh, H.E., Ghanem, S.S., Al-Share, Q.Y., Smiley, Z.N., Gatto-Weis, C., et al., 2016. Role for hepatic CEACAM1 in regulating fatty acid metabolism along the adipocyte-hepatocyte axis. *The Journal of Lipid Research* 57(12):2163–2175. <https://doi.org/10.1194/jlr.M072066>. PubMed PMID: 27777319; PMCID: PMC5321226.
- [38] Janowski, B.A., Willy, P.J., Devi, T.R., Falck, J.R., Mangelsdorf, D.J., 1996. An oxysterol signalling pathway mediated by the nuclear receptor LXR alpha. *Nature* 383(6602):728–731. <https://doi.org/10.1038/383728a0>. PubMed PMID: 8878485.
- [39] Park, K., Scott, A.L., 2010. Cholesterol 25-hydroxylase production by dendritic cells and macrophages is regulated by type I interferons. *Journal of Leukocyte Biology* 88(6):1081–1087. <https://doi.org/10.1189/jlb.0610318>. PubMed PMID: 20699362; PMCID: PMC2996899.
- [40] Wentworth, J.M., Naselli, G., Brown, W.A., Doyle, L., Phipson, B., Smyth, G.K., et al., 2010. Pro-inflammatory CD11c+CD206+ adipose tissue macrophages are associated with insulin resistance in human obesity. *Diabetes* 59(7): 1648–1656. <https://doi.org/10.2337/db09-0287>. PubMed PMID: 20357360; PMCID: PMC2889764.
- [41] Guillemot-Legris, O., Mutemberezi, V., Cani, P.D., Muccioli, G.G., 2016. Obesity is associated with changes in oxysterol metabolism and levels in mice liver, hypothalamus, adipose tissue and plasma. *Scientific Reports* 6:19694. <https://doi.org/10.1038/srep19694>. PubMed PMID: 26795945; PMCID: PMC4726335.
- [42] Wyss, A., Raselli, T., Perkins, N., Ruiz, F., Schmelzger, G., Klinke, G., et al., 2019. The EBI2-oxysterol axis promotes the development of intestinal lymphoid structures and colitis. *Mucosal Immunology* 12(3):733–745. <https://doi.org/10.1038/s41385-019-0140-x>. PubMed PMID: 30742043.
- [43] Adams, C.M., Reitz, J., De Brabander, J.K., Feramisco, J.D., Li, L., Brown, M.S., et al., 2004. Cholesterol and 25-hydroxycholesterol inhibit activation of SREBPs by different mechanisms, both involving SCAP and Insigs. *Journal of Biological Chemistry* 279(50):52772–52780. <https://doi.org/10.1074/jbc.M410302200>. PubMed PMID: 15452130.
- [44] Dong, X.Y., Tang, S.Q., Chen, J.D., 2012. Dual functions of Insig proteins in cholesterol homeostasis. *Lipids in Health and Disease* 11:173. <https://doi.org/10.1186/1476-511X-11-173>. PubMed PMID: 23249523; PMCID: PMC3564778.
- [45] Ecker, J., Liebis, G., Englmaier, M., Grandl, M., Robenek, H., Schmitz, G., 2010. Induction of fatty acid synthesis is a key requirement for phagocytic differentiation of human monocytes. *Proceedings of the National Academy of Sciences of the United States of America* 107(17):7817–7822. <https://doi.org/10.1073/pnas.0912059107>. PubMed PMID: 20385828; PMCID: PMC2867858.
- [46] Prunet, C., Montange, T., Vejux, A., Laubriet, A., Rohmer, J.F., Riedinger, J.M., et al., 2006. Multiplexed flow cytometric analyses of pro- and anti-inflammatory cytokines in the culture media of oxysterol-treated human monocytic cells and in the sera of atherosclerotic patients. *Cytometry, Part A* 69(5):359–373. <https://doi.org/10.1002/cyto.a.20272>. PubMed PMID: 16604541.
- [47] Koarai, A., Yanagisawa, S., Sugiura, H., Ichikawa, T., Kikuchi, T., Furukawa, K., et al., 2012. 25-Hydroxycholesterol enhances cytokine release and Toll-like receptor 3 response in airway epithelial cells. *Respiratory Research* 13:63. <https://doi.org/10.1186/1465-9921-13-63>. PubMed PMID: 22849850; PMCID: PMC3460764.
- [48] Reboldi, A., Dang, E.V., McDonald, J.G., Liang, G., Russell, D.W., Cyster, J.G., 2014. Inflammation. 25-Hydroxycholesterol suppresses interleukin-1-driven inflammation downstream of type I interferon. *Science* 345(6197):679–684. <https://doi.org/10.1126/science.1254790>. PubMed PMID: 25104388; PMCID: PMC4289637.
- [49] Rosklint, T., Ohlsson, B.G., Wiklund, O., Noren, K., Hulthen, L.M., 2002. Oxysterols induce interleukin-1beta production in human macrophages. *European Journal of Clinical Investigation* 32(1):35–42. <https://doi.org/10.1046/j.1365-2362.2002.00931.x>. PubMed PMID: 11851725.
- [50] Englund, M.C., Karlsson, A.L., Wiklund, O., Bondjers, G., Ohlsson, B.G., 2001. 25-hydroxycholesterol induces lipopolysaccharide-tolerance and decreases a lipopolysaccharide-induced TNF-alpha secretion in macrophages. *Atherosclerosis* 158(1):61–71. PubMed PMID: 11500175.
- [51] Wiesner, P., Choi, S.H., Almazan, F., Benner, C., Huang, W., Diehl, C.J., et al., 2010. Low doses of lipopolysaccharide and minimally oxidized low-density lipoprotein cooperatively activate macrophages via nuclear factor kappa B

and activator protein-1: possible mechanism for acceleration of atherosclerosis by subclinical endotoxemia. *Circulation Research* 107(1):56–65. <https://doi.org/10.1161/CIRCRESAHA.110.218420>. PubMed PMID: 20489162; PMCID: PMC2904601.

[52] Choi, S.H., Wiesner, P., Almazan, F., Kim, J., Miller, Y.I., 2012. Spleen tyrosine kinase regulates AP-1 dependent transcriptional response to minimally oxidized LDL. *PloS One* 7(2):e32378. <https://doi.org/10.1371/journal.pone.0032378>. PubMed PMID: 22384232; PMCID: PMC3284564.